Available online at www.sciencedirect.com
ScienceDirect
Journal of Sound and Vibration 324 (2009) 179–193
JOURNAL OF SOUND AND VIBRATION
www.elsevier.com/locate/jsvi

Lateral vibration of a composite stepped beam consisted of SMA helical spring based on equivalent Euler–Bernoulli beam theory

Chun-Ying Lee[a,*], Huan-Chang Zhuo[b], Chia-Wei Hsu[b]

[a]*Department of Mechanical Engineering, National Taipei University of Technology, Taipei 106, Taiwan*
[b]*Department of Mechanical and Automation Engineering, Da-Yeh University, Da-Tsuen, Changhua 515, Taiwan*

Received 5 December 2007; received in revised form 24 November 2008; accepted 31 January 2009
Handling Editor: L.G. Tham
Available online 3 March 2009

Abstract

The dynamic characteristics of the shape memory alloy (SMA) helical spring proposed to be used in the semi-active suspension platform (e.g. the optic disk drive) are considered in this study. The component mounted on the platform generates periodic oscillation due to parametric excitation, such as rotation of an eccentric mass. In this way, the induced vibration of the platform could load the suspension spring in both axial and lateral directions. Besides its tunable dynamic characteristics by phase transformation, the SMA helical spring providing both axial and lateral flexibilities is applicable in this regards. In this paper, the spring constant of the helical spring in transverse deformation was first derived by employing the first theorem of Castigliano's. The derived spring constant was then used to define the equivalent flexural stiffness of the spring. Consequently, the natural frequency of a stepped composite beam with the assembly of SMA spring and other beam-like component was derived by transfer matrix method. The calculated natural frequencies of the stepped beam were compared with the experimental measurements. It is found that the formulation well predicted the natural frequency of the SMA spring both in martensite and austenite phases, respectively. The tunable characteristics of the SMA helical spring in lateral vibration were also demonstrated.

1. Introduction

The increasing demand for the high-precision and excellent-performance machinery has offered engineers challenges in suppression of vibration. For example, the pursuit of higher and higher read/write speed of optical disk drive has rendered the solutions of a variety of vibration suppression techniques. For an optic disk drive platform with imbalanced mass, the centrifugal force generated by the high speed rotation of the disk induces the vibration of the platform. For the common practice, the suspension springs consist of metallic spring washer or rubber ring. The dynamic characteristics of the washer can be optimally tuned for certain operation conditions to minimize the induced vibration. However, the disk drive usually reads or writes in different speeds. Thus, the tuning of the washer becomes difficult for minimizing the vibration in all operational conditions.

*Corresponding author. Tel.: +886 2 27712171; fax: +886 2 27317191.
E-mail address: leech@ntut.edu.tw (C.-Y. Lee).

0022-460X/$ - see front matter © 2009 Elsevier Ltd. All rights reserved.
doi:10.1016/j.jsv.2009.01.055

Another category of vibration reduction device used in the commercial optic disk drive is the ball balancer [1–3]. Basically, the freely movable balls in the circular tracks are automatically driven to their counterbalance positions which center of mass is in 180-degree, opposite side, to the imbalanced mass. These balls generate counterbalance force to cancel the centrifugal force caused by the imbalanced mass. The induced vibration is therefore reduced. However, the ball balancer device only works when the rotation speed exceeds the critical speed of the platform. It will not reduce the vibration if the rotational speed is lower than the natural frequency of the platform [1,4]. Therefore, the semi-active tuning of this platform's fundamental frequency would benefit the robustness in this vibration control strategy.

Along with other smart materials, shape memory alloy (SMA) can change its material properties under the influence of control parameter. For instance, electrorheological (ER) fluid undergoes phase transition from viscous liquid to Bingham plastic with the application of electric field. The idea of using suspension washer with embedded ER fluid for the optic disk drive platform was demonstrated to be capable of tuning the platform's natural frequency with applied electric field [5]. On the other hand, the Young's modulus of the SMA increases from martensite to austenite with the actuation of heat and/or strain. This tunable characteristic makes SMA a viable candidate for the application in semi-active vibration control. Some examples of employing the tunable property of the SMA in the literature are as follows: the composite beam with embedded SMA wires [6], the vibration absorber in the form of cantilever SMA beam [7] and the compression helical spring [8], etc. Although the application of SMA spring has been discussed in the semi-active vibration control, the spring washer used in the optic disk drive platform for the same purpose is new. The helical spring provides the suspension joint with six degrees of freedom to deform. Among the six degrees of freedom, transverse deflections and rotations in two perpendicular directions are four of them while the axial deformation and axial twisting are the remaining two. The helical spring in this application is subjected to transverse deformation in contrast to axial or twisting deformation for usual designs.

In the three-dimensional, dynamic analysis of helical springs, the governing equations become 12 simultaneous partial differential equations with inertia terms. Finding the closed-form solution is very difficult [9]. Numerical methods are ordinarily employed for some specific cases, e.g. finite element method [10], transfer matrix method [11], pseudospectral method [12]. Therefore, to simplify the helical spring model and consider only the lateral deformation, the spring constant of a helical spring in transverse loading was first formulated in this study using the first theorem of Castigliano's. The spring constant was then employed to obtain an equivalent flexural stiffness of the helical spring. The helical spring can be regarded as a segment with equivalent flexural stiffness within a composite stepped beam, where the other segments resemble the suspended component. The natural frequency of the assembly beam was formulated. Experimental measurement was finally conducted to validate the theoretical formulations.

2. Theoretical formulation

Since only the lateral vibration of helical spring is considered in this study, the spring subjecting to transverse force and bending moment is schematically shown in Fig. 1. The axial loading and twisting moment to helical spring cylinder are omitted accordingly. Fig. 1 illustrates the geometric configuration and associate end loadings $\boldsymbol{F_0}$ and $\boldsymbol{M_0}$ of the helical spring. p is the pitch, R is the mean helical radius, L_0 is the axial free length and θ is the polar coordinate of the spring. The assumptions used in this study were summarized as following:

(1) The material is isotropic and deformed within its linearly elastic range.
(2) The wire of the helical spring is in circular cross-section and no warping occurs during twisting deformation.
(3) Compared with the mean diameter of the helix, the wire diameter is small. The curvature effect on the stress distribution of the cross-section can be neglected.
(4) The deformation is small in nature. Thus, the first theorem of Castigliano's can be used to derive the spring constant of the linear spring.
(5) Only the bending vibration of the composite stepped beam is considered, i.e. the Euler–Bernoulli beam theory can be applied.

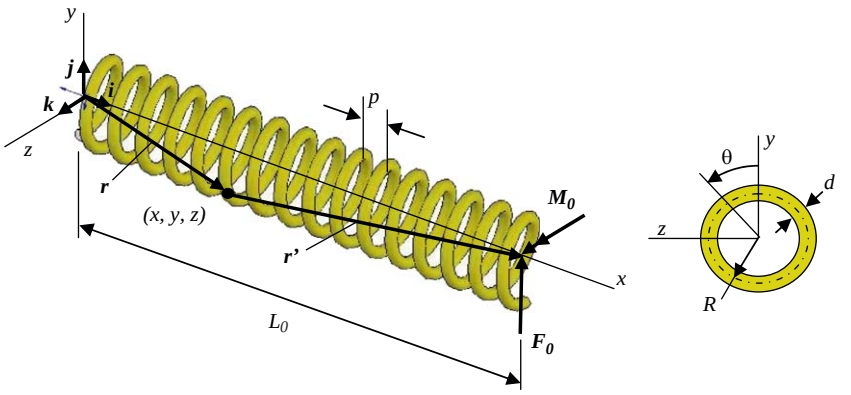

Fig. 1. Schematic configuration of a helical spring subjected to lateral loadings, $\boldsymbol{F_0}$ and $\boldsymbol{M_0}$, at the end.

The position vector of the centroid at a cross section of the helical spring with right-hand helix can be expressed as:

$$\vec{r} = x\,\vec{i} + y\,\vec{j} + z\,\vec{k}, \tag{1}$$

where $x = (\theta/2\pi)p$, $y = R\cos\theta$, $z = R\sin\theta$.

If a left-hand helix is considered, the axial pitch p will be a negative value. By taking the derivatives of the above coordinates with respect to θ, we can find the unit tangent vector of the helical line:

$$\vec{e}_t \equiv \frac{\mathrm{d}\vec{r}}{|\mathrm{d}\vec{r}|} = \frac{\mathrm{d}x\,\vec{i} + \mathrm{d}y\,\vec{j} + \mathrm{d}z\,\vec{k}}{\sqrt{\mathrm{d}x^2 + \mathrm{d}y^2 + \mathrm{d}z^2}} = \frac{1}{\ell}\left(\frac{p}{2\pi}\,\vec{i} - R\sin\theta\,\vec{j} + R\cos\theta\,\vec{k}\right). \tag{2}$$

In the above equation, the wire length per unit radian angle $\sqrt{R^2 + (p/2\pi)^2}$ was denoted as ℓ to simplify the expression in the following derivations. The equivalent force and couple at the centroid of the cross-section (x, y, z) can be written as:

$$\vec{F} = F_0\,\vec{j}, \tag{3a}$$

$$\vec{M} = \vec{r}' \times \vec{F}_0 + M_0\,\vec{k}, \tag{3b}$$

where $\vec{r}'$ is the moment arm vector of the external force relative to the cross-section at (x, y, z), as following:

$$\vec{r}' = \left(L_0 - \frac{p}{2\pi}\theta\right)\vec{i} - R\cos\theta\,\vec{j} - R\sin\theta\,\vec{k}. \tag{4}$$

Accordingly, the reaction force in Eq. (3a) can be resolved into axial and transverse components P and V, which are axial force and shear force in the spring wire, respectively. Similarly, the moment in Eq. (3b) can be resolved into twisting torque T and bending moment M in the wire:

$$P = \vec{F}\cdot\vec{e}_t, \quad V = \sqrt{|\vec{F}|^2 - P^2}, \tag{5a}$$

$$T = \vec{M}\cdot\vec{e}_t, \quad M = \sqrt{|\vec{M}|^2 - T^2}. \tag{5b}$$

Under the assumption of using wire with circular cross-section and linear deformation, the total strain energy U can be obtained by integrating the strain energy density associated with the above four internal reactions over the length of the wire:

$$U = \int_0^{\Theta}\left(\frac{M^2}{2EI} + \frac{T^2}{2GJ} + \frac{P^2}{2EA} + \frac{\alpha V^2}{2GA}\right)\ell\,d\theta. \tag{6}$$

In the above equation, $\Theta = 2\pi N_c$, N_c denotes the total number of active coils of the spring and α is shear correction factor for the wire cross-section. Because the wire with circular cross-section is considered, α is

taken to be 1.333 herein [13]. A, I and J are the cross-sectional area, central quadratic moment and quadratic moment of torsion of the spring wire, respectively. The material properties are denoted by the Young's modulus E and shear modulus G.

2.1. Pure bending without lateral force at the spring end

With $F_0 = 0$, the internal axial force P and shear force V vanish. The twisting moment and bending moment in the wire, as noted in Eq. (5b), can be expressed as:

$$T = \frac{M_0 R\cos\theta}{\ell}, \quad M = \frac{M_0\sqrt{\ell^2 - R^2\cos^2\theta}}{\ell}. \tag{7}$$

And, the associated strain energy U can be obtained by calculating the integration of Eq. (6). The end rotation θ_0 can then be found by employing the first theorem of Castigliano's:

$$\theta_0 = \frac{\partial U}{\partial M_0}. \tag{8}$$

The associated spring constant for the spring subjected to end moment can thus be derived as:

$$k \equiv \frac{M_0}{\theta_0} = \left\{\frac{1}{EI\ell}\left[\left(\ell^2 - \frac{R^2}{2}\right)\Theta - \frac{R^2}{4}\sin(2\Theta)\right] + \frac{R^2}{GJ\ell}\left(\frac{\Theta}{2} + \frac{\sin(2\Theta)}{4}\right)\right\}^{-1}. \tag{9}$$

If this spring constant results an equivalent cantilever beam with an end moment M_0 and axial free length of the cylinder $L_0 = N_c p$, the equivalent flexural stiffness of the helical spring can be obtained:

$$(EI)_{eq} = kL_0. \tag{10}$$

2.2. Simple lateral force at the spring free end

In this loading, $M_0 = 0$. The equivalent reactions of the cross-section at (x, y, z) can be found from the equilibrium conditions and Eqs. (5a,b) as follows:

$$P = -\frac{R\sin\theta}{\ell}F_0, \quad V = \frac{\sqrt{\ell^2 - R^2\sin^2\theta}}{\ell}F_0 \tag{11}$$

$$T = \left[\frac{pR}{2\pi\ell}\sin\theta + \left(L_0 - \frac{p}{2\pi}\right)\frac{R}{\ell}\cos\theta\right]F_0 \tag{12a}$$

$$M = \left\{\left(L_0 - \frac{p}{2\pi}\theta\right)^2 + R^2\sin^2\theta - \left[\frac{pR}{2\pi\ell}\sin\theta + \left(L_0 - \frac{p}{2\pi}\theta\right)\frac{R}{\ell}\cos\theta\right]\right\}^{1/2}F_0 \tag{12b}$$

The strain energy can be calculated by substituting these internal forces and moments into Eq. (6). Consequently, the end deflection δ can also be found by employing the first theorem of Castigliano's:

$$\delta = \frac{\partial U}{\partial F_0}. \tag{13}$$

The derived spring constant can be written as:

$$\begin{aligned} k \equiv \frac{F_0}{\delta} = \Bigg\{ & \frac{\alpha\ell}{GA}\Theta + \left(\frac{1}{EA} - \frac{\alpha}{GA}\right)\frac{R^2}{\ell}\left(\frac{\Theta}{2} - \frac{\sin 2\Theta}{4}\right) + \frac{\ell}{EI}\left[\left(1 - \frac{p^2}{4\pi^2\ell^2}\right)\frac{R^2}{2}\Theta - \frac{R^2}{4}\sin 2\Theta + \left(1 - \frac{R^2}{2\ell^2}\right)\frac{2\pi}{3p}L_0^3\right] \\ & + \frac{1}{GJ}\left[\frac{p^2R^2}{8\pi^2\ell}\Theta + \frac{\pi R^2 L_0^3}{3p\ell}\right] + \left(\frac{1}{GJ} - \frac{1}{EI}\right)\left[\left(\frac{R^2L_0^2}{4\ell} - \frac{5p^2R^2}{32\pi^2\ell}\right)\sin 2\Theta + \frac{pR^2L_0}{8\pi\ell}(3 - 3\cos 2\Theta - 2\Theta\sin 2\Theta)\right. \\ & \left. + \frac{p^2R^2}{16\pi^2\ell}(3\Theta\cos 2\Theta + \Theta^2\sin 2\Theta)\right]\Bigg\}^{-1} \end{aligned} \tag{14}$$

If this spring constant is the consequence of an equivalent cantilever beam with an end force F_0 and length $L_0 = N_c p$, the equivalent flexural stiffness of the helical spring can be obtained:

$$(EI)_{eq} = k\frac{L_0^3}{3}. \tag{15}$$

2.3. Simple lateral force at the end with restrained rotation

This is a statically indeterminate problem with the end reactions shown in Fig. 1, where the moment M_0 is the reaction for keeping the end un-rotated under the applied end force F_0. This configuration occurs when the platform above the suspension spring is free to transverse displacement with prohibited rotation. Hence, with the axial force and transverse shear reactions described in Eqs. (5a), the same results as those in Eqs. (11) can be obtained. The twisting and bending moments described in Eqs. (5b) become:

$$T = \frac{pRF_0}{2\pi\ell}\sin\theta + \left[M_0 + \left(L_0 - \frac{p}{2\pi}\right)F_0\right]\frac{R}{\ell}\cos\theta \tag{16a}$$

$$M = \left\{\left[M_0 + \left(L_0 - \frac{p}{2\pi}\theta\right)F_0\right]^2 + F_0^2R^2\sin^2\theta - \left[\frac{pRF_0}{2\pi\ell}\sin\theta + \left(M_0 + \left(L_0 - \frac{p}{2\pi}\theta\right)F_0\right)\frac{R}{\ell}\cos\theta\right]^2\right\}^{1/2}, \tag{16b}$$

With these reactions at the cross-section of the wire, the strain energy can be calculated by the integration in Eq. (6). Because the end of the spring is constrained in angular rotation ($\theta_0 = 0$), the following equation can be written by adopting the first theorem of Castigliano's:

$$\theta_0 = \frac{\partial U}{\partial M_0} = 0. \tag{17}$$

Eq. (17) is the equation relating the reactive moment M_0 to the applied loading F_0 at the end of the spring. The above equation can be written explicitly as:

$$M_0 = QF_0, \tag{18}$$

where

$$Q = \left\{\frac{1}{EI}\left(\frac{p}{4\pi}\Theta^2 - L_0\Theta\right) - \left(\frac{1}{GJ} - \frac{1}{EI}\right)\left[\frac{R^2L_0}{4\ell^2}(2\Theta + \sin 2\Theta) + \frac{pR^2}{16\pi\ell^2}(3 - 3\cos 2\Theta - 2\Theta^2 - 2\Theta\sin 2\Theta)\right]\right\} \Big/ \left[\frac{\Theta}{EI} + \left(\frac{1}{GJ} - \frac{1}{EI}\right)\frac{R^2}{\ell^2}\left(\frac{\Theta}{2} + \frac{\sin 2\Theta}{4}\right)\right].$$

Substituting the resulted relationship back into Eqs. (16) and using the first theorem of Castigliano's Eq. (13) again, we can derive the lateral deflection of the spring at the end and the spring constant can be obtained subsequently:

$$\begin{aligned} k \equiv \frac{F_0}{\delta} = \Bigg\{ & \frac{\alpha\ell}{GA}\Theta + \left(\frac{1}{EA} - \frac{\alpha}{GA}\right)\frac{R^2}{\ell}\left(\frac{\Theta}{2} - \frac{\sin 2\Theta}{4}\right) \\ & + \frac{\ell}{EI}\left[\left(\frac{R^2}{2} + (Q + L_0)^2\right)\Theta - \frac{R^2}{4}\sin 2\Theta + (Q + L_0)\frac{p}{2\pi}\Theta^2 + \frac{p^2}{12\pi^2}\Theta^3\right] \\ & + \left(\frac{1}{GJ} - \frac{1}{EI}\right)\left[\frac{p^2R^2}{32\pi^2\ell}\left(4\Theta - 5\sin 2\Theta + \frac{4}{3}\Theta^3 + 2\Theta^2\sin 2\Theta + 6\Theta\cos 2\Theta\right)\right. \\ & + \frac{pR^2}{8\pi\ell}(Q + L_0)(3 - 3\cos 2\Theta - 2\Theta\sin 2\Theta - 2\Theta^2) \\ & \left. + \frac{R^2}{4\ell}(Q + L_0)^2(2\Theta + \sin 2\Theta)\right]\Bigg\}^{-1} \end{aligned} \tag{19}$$

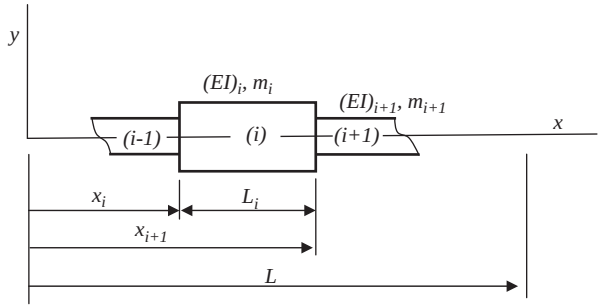

Fig. 2. Schematic diagram of a stepped beam.

When this spring constant results from an equivalent cantilever beam with an end force F_0 and restrained end rotation, the equivalent flexural stiffness of the helical spring can be obtained:

$$(EI)_{eq} = k\frac{L_0^3}{12}. \tag{20}$$

2.4. Natural frequency of a stepped composite beam

The SMA helical spring used in the semi-active suspension and even the active vibration control must connect to the other part of the structure. For simplicity, the helical spring is modeled as an equivalent uniform beam with the derived sectional properties in the previous sections, and the connection to other beam-like components is considered herein. It can also be imagined as a robot arms with structural members interconnected at the joints with SMA helical spring actuators. Fig. 2 presents the schematic diagram of a stepped beam. In this figure, each segment represented by the equivalent cross-sectional properties can be an ordinary beam or an equivalent beam of the helical spring derived from the previous formulation. The transfer matrix method [14–16] was adopted herein in the solution process. The detail formulation of this solution process can be seen in the Appendix A.

3. Experimental setup

The SMA spring used in this study was a commercial product distributed by Jameco Electronics. The mean diameter of the coil and the diameter of the wire are 7.3 and 1 mm, respectively. The mass density of the SMA wire is 6400 kg m^{-3}. Due to the unavailability of the material property, an axial loading testing apparatus was set up to study the phase transformation characteristics of the SMA spring, as shown schematically in Fig. 3. The SMA spring was loaded between two Teflon insulating spacers. The insulating spacers confined the electric current to the spring only and thus raised its temperature via ohmic effect. A control module controlled the current supply and the temperature was monitored by a thermocouple. As for the measurement of mechanical loading and the associate deflection, the deflection was imposed by adjusting the clamped length of the micrometer while the serial connected load cell kept recording the corresponding compressive loading. The slope of the measured load-deflection curve provided the rate of the spring at various controlled temperatures.

The measured spring constant of the axially loaded SMA spring was employed to inferred the equivalent Young's modulus from the design formula of helical spring $k = Gd^4/64R^3N_c$ and $E = 2(1+\nu)G$. The Poisson's ratio ν was taken to be 0.3. Before any measurement started, the SMA spring was quenched in the liquid nitrogen to fully recover to the martensitic phase. As the temperature was raised to 90 °C, the phase transformation from martensite to austenite would be completed and the SMA was in the austenite phase. The moduli of the SMA at these two phases were calculated, respectively. It was found that Young's modulus of the SMA was 34.2 GPa at room temperature while 68.5 GPa at 90 °C.

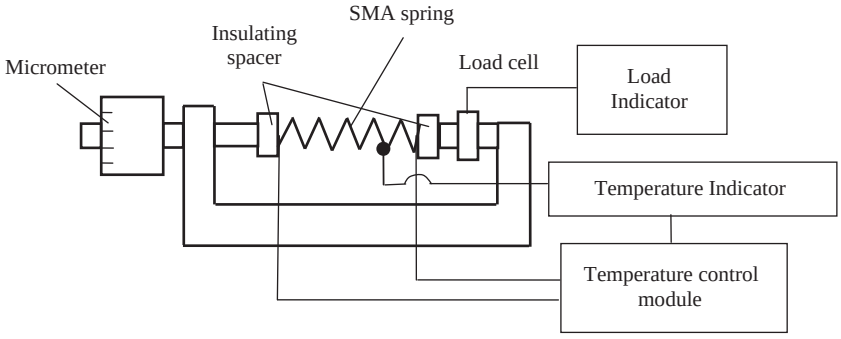

Fig. 3. Schematic diagram of the apparatus for static testing of axially loaded SMA spring.

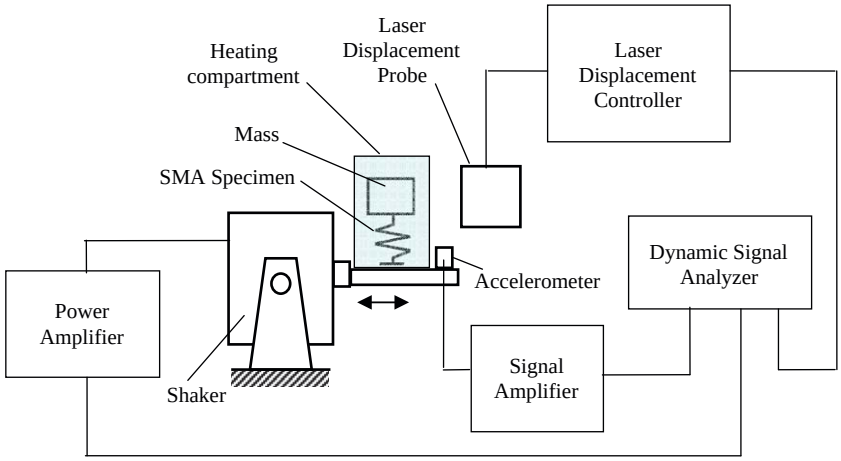

Fig. 4. The schematic diagram of the test apparatus for dynamic measurement of SMA spring–mass system in transverse vibration.

The dynamic characteristics of the SMA spring in transverse vibration were investigated using the experimental setup shown schematically in Fig. 4. The spring–mass system was excited in base vibration by a mechanical shaker. The excitation was measured by the accelerometer mounted on the base while the resulted vibration displacement of the mass was detected by the laser displacement probe. Both the mass displacement and the base vibration were processed by the dynamic signal analyzer to find the resonance frequency of the system. The temperature of the spring was controlled by the heating compartment encasing the system. The dynamic characteristics of the system were measured while the SMA spring was at the martensite and the austenite phases, respectively. Because the SMA spring was intended to be used in the switching between the martensite and austenite phases, the state at the incomplete transformation was not investigated herein.

4. Results and discussions

Before we proceeded to the SMA spring, a steel helical spring with $d = 1\,\text{mm}$, $R = 4.25\,\text{mm}$, and $p = 3.86\,\text{mm}$ was tested in fixed-free, i.e. cantilever, boundary condition. Because the steel has more stable material property (Young's modulus 210 GPa, mass density 7800 kg m^{-3}), that is not subjected to the influence of phase transformation at low temperature and stress as compared with its SMA counterpart, this measurement can be employed to verify the formulation of this study. Fig. 5 presents the first two modes' natural frequencies of this steel spring in different spring lengths. The theoretical results were obtained by treating the spring as an equivalent uniform beam as in the previous formulation. The natural frequencies decrease rapidly as the spring becomes longer in length. The results in Fig. 5 show that the present predictions

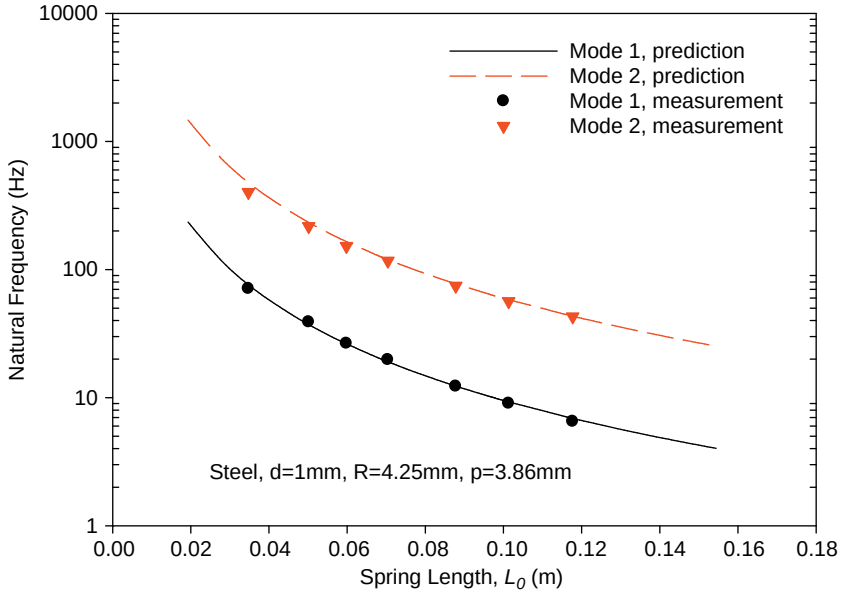

Fig. 5. The first two modes' natural frequencies of a cantilever helical steel spring under transverse vibration.

correlate very well with the measurements. Another example used to validate the formulation of this study was a benchmark problem presented by Mottershead [10]. The results shown in Table 1 are the first two natural frequencies of a helical spring with fixed-fixed boundary conditions, which correspond to lateral vibration modes. The frequency results of the present equivalent beam model give the same value in the two lateral directions while they are different in 3-D formulations [9,10]. The deficiency of our formulation is mainly due to the equivalent beam model adopted for the helical spring. When a beam model with same cross-sectional properties in the lateral directions is assumed, no distinction can be made between these two lateral axes. Nevertheless, the present prediction is within 3% difference with those of 3-D formulations.

The use of the first steel spring in suspension was simulated by attaching a piece of solid steel rod to the tip of the spring. The steel end piece was 7.5 mm in diameter and 14 mm in length. Both the prediction and measurement of the fundamental natural frequency are presented in Fig. 6. It is clearly seen that the natural frequency of this composite stepped beam is well predicted for the suspension spring in different lengths. The associated mode shapes of this composite beam assembly with spring length 20 mm were calculated and shown in Fig. 7. Because the flexural stiffness of the solid steel rod is higher than that of the helical spring, most bending deflection occurs in the helical spring segment.

With the validated formulation from the previous examples, the effect of the configuration parameters on the equivalent property of the spring was investigated numerically. Fig. 8 presents the change of the spring constant with the spring length and the equivalent flexural stiffness of the SMA spring in different transverse loadings and end conditions. It is obviously seen that the spring constant decreases rapidly as the spring becomes longer in axial length. Furthermore, as expected, the spring with ends restrained in rotations demonstrates higher rigidity. Although the numerical value of the spring constant for the spring subjected to end moment was several orders smaller than its other counterparts in different boundary conditions, it must be noted that the definitions for the spring constants are different as described in Eqs. (9) and (14). The equivalent flexural stiffness shows a different trend. When a short spring was loaded, the contribution in deflection due to the transverse force was significant as compared with its moment counterparts. This adds on to the deflection by the moments. The influence direct from the transverse force diminishes as the spring becomes longer in length and, consequently, the moments dominate the overall deflection. Consequently, the springs of different lengths under end moment show little change in equivalent flexural stiffness except when the spring is with very few number of coils, e.g. less than two coils. In addition, the equivalent flexural stiffness for both the end force loadings approaches the other one with end moment.

Table 1
The natural frequencies (Hz) of a helical spring made of an isotropic material and with two fixed ends: $\rho = 7900\,\mathrm{kg\,m^{-3}}$, $E = 206.1\,\mathrm{GPa}$, $v = 0.3$, $R = 5\,\mathrm{mm}$, $d = 1\,\mathrm{mm}$, $p = 4.737\,\mathrm{mm}$, $L_0 = 36\,\mathrm{mm}$.

Mode	Mottershead [10]	Yildirim [9]	Present
ω_1	396	394	405
ω_2	397	396	405

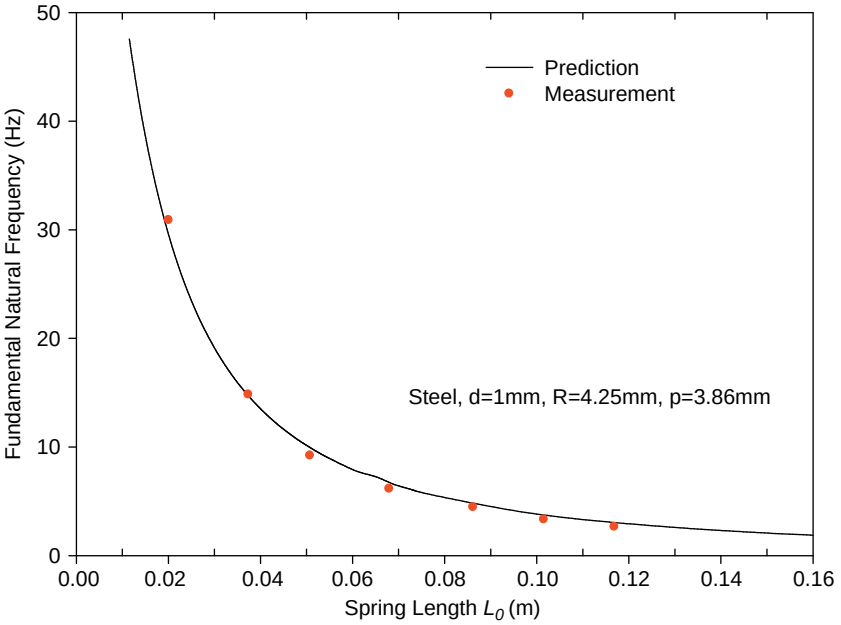

Fig. 6. The fundamental natural frequency of a stepped beam with a solid steel rod suspended on top of the steel helical spring.

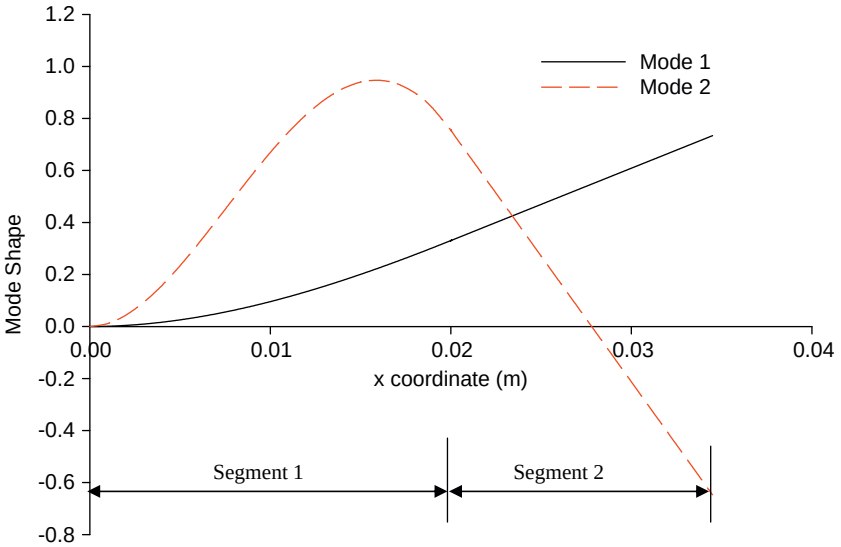

Fig. 7. The simulated results of the first two mode shapes of a stepped beam with a solid steel rod suspended on top of the steel helical spring.

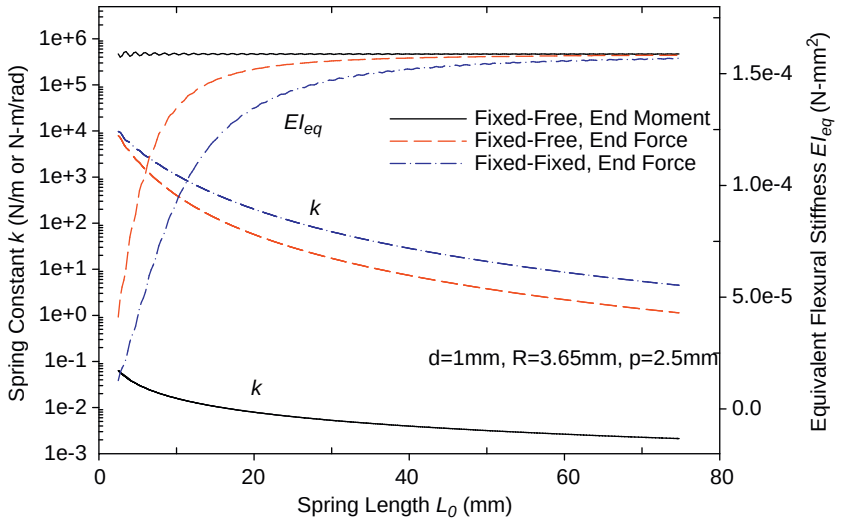

Fig. 8. The spring constants and equivalent flexural stiffness of the helical SMA springs with $d = 1\,\text{mm}$, $R = 3.65\,\text{mm}$, $p = 2.5\,\text{mm}$.

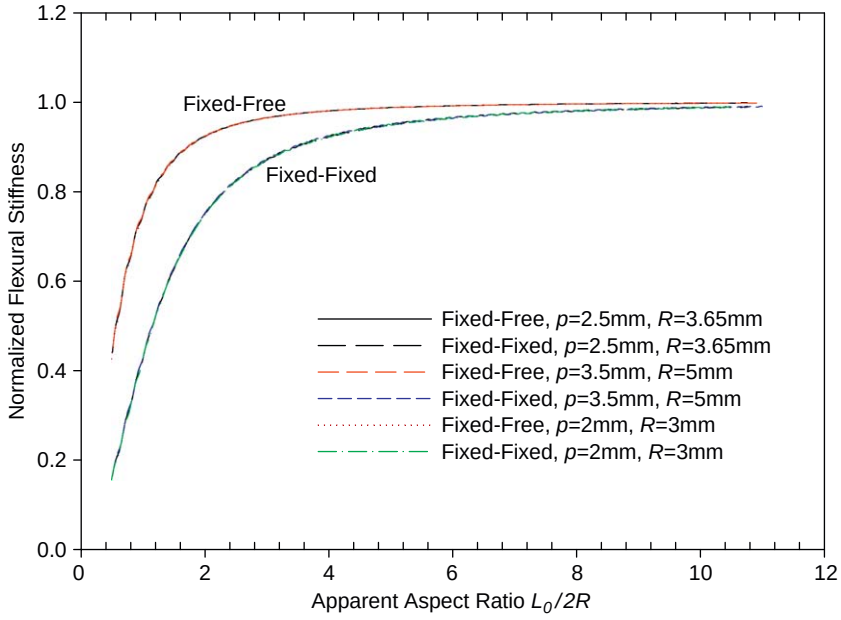

Fig. 9. The normalized flexural stiffness corresponding to the apparent aspect ratio of the helical SMA springs.

The effect of spring dimensions on the equivalent flexural stiffness can be illustrated in Fig. 9. For the springs of several different pitches and helical diameters, the flexural stiffness is normalized with respect to its corresponding one in simple end moment bending. The apparent aspect ratio was denoted as the ratio of spring length to mean helical diameter. For the different configurations studied, the results in Fig. 9 show that, as the apparent aspect ratio is larger than 6, the normalized flexural stiffness reaches 0.95. In other words, the use of Eq. (10) to estimate the flexural stiffness of the helical spring will be within 5% of accuracy.

Fig. 10 presents the prediction of the fundamental natural frequency of the cantilever SMA helical spring in different lengths. The free end of the spring had no attachment and the spring was a uniform beam. Therefore, the transfer matrix $[T]$ in Eq. (A.8) would be an identity matrix. The singularity of $[T_R]$ in Eq. (A.15) can be

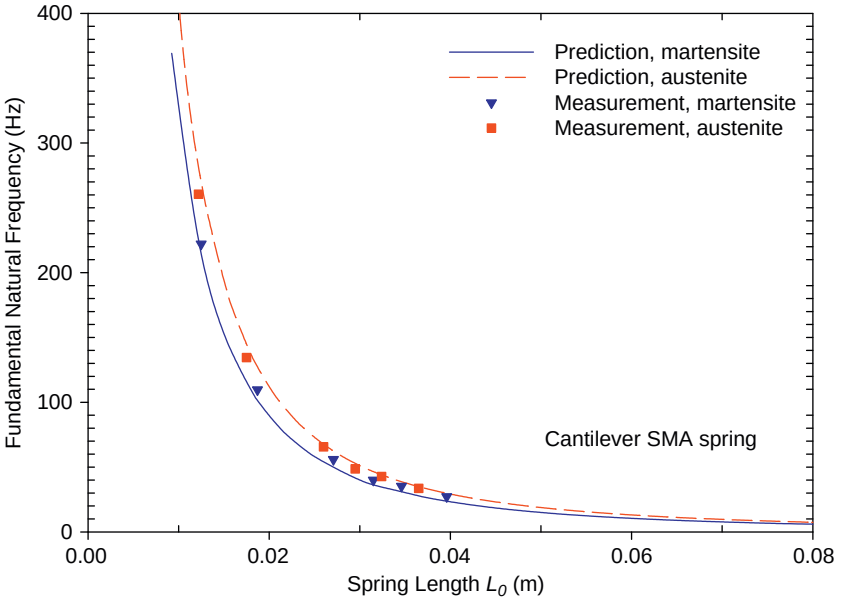

Fig. 10. The fundament natural frequencies of the cantilever SMA helical spring at martensite and austenite phases.

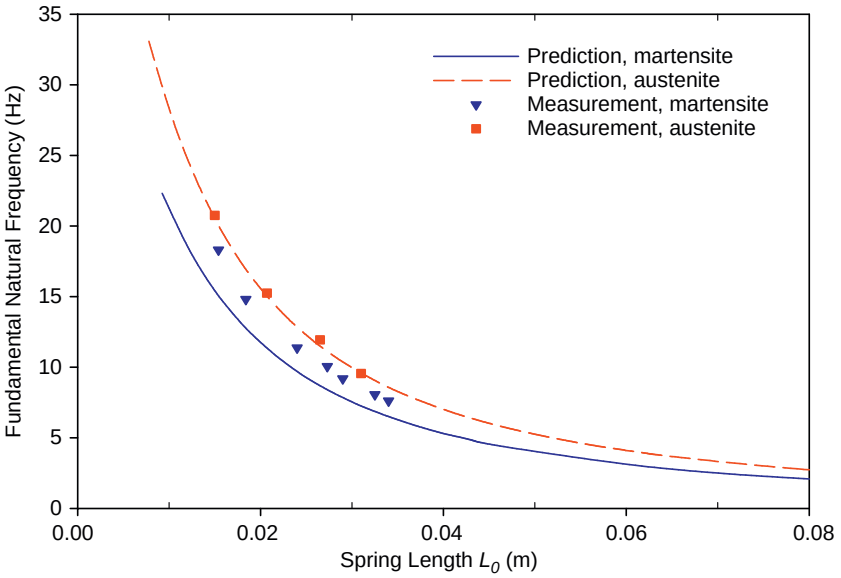

Fig. 11. The fundamental natural frequency of an assembly system with solid steel rod suspended on top of the SMA helical spring.

used to find the λ_1, and consequently ω through Eq. (A.3). Because of the limited length of the purchased SMA spring, only the natural frequencies of the spring at six different lengths were measured at both martensite and austenite states, respectively. The spring demonstrates a raise in natural frequency from the martensite to the austenitic phase. It is obvious that prediction and measurement are in good agreement.

The system of SMA spring in a suspension platform was simulated as a solid rod attached to the end of a SMA spring, similar to those performed in Fig. 6. The fundamental natural frequency of this two-segment stepped beam was studied. The same end piece, i.e. a solid steel rod with diameter 7.5 mm and length 14 mm, was used. Fig. 11 presents the fundamental natural frequency of the system with the suspension spring in martensite and austenite phases, respectively. The simulation fairly predicted the trend and change in the

fundamental natural frequency of the system. Applying the static material property to dynamic environment for the SMA material could result in the discrepancy in the magnitude of the frequency at martensitic phase.

5. Conclusions

The change of the dynamic characteristics of the transversely loaded SMA helical spring due to the martensite–austenite transformation was investigated in this study. The theoretical formulation of treating the helical spring as an equivalent uniform beam was validated by the measurement of the natural frequency of a steel spring in transverse vibration. Furthermore, the use of Euler–Bernoulli beam theory simplifies the formulation compared with those of 3-D model in the literature. The equivalent flexural stiffness was found to approach, within 5% difference, the one under simple transverse bending as the apparent aspect ratio of the helical spring was greater than six. In other words, the laterally loaded helical spring can be regarded as a uniform beam with the equivalent flexural stiffness for intermediate and long springs. Finally, the fundamental frequency of a stepped composite beam with the incorporation of the helical spring as the suspension element was also formulated using transfer matrix method. The predicted natural frequency of the system with a component on top of the SMA spring matched the experimental measurement very well. The modeling of the suspension platform with multiple suspension springs using the derived formulation can be the topics for further study.

Acknowledgement

The financial support from NSC, Taiwan, under the Grant No. NSC 95-2221-E-212-004-MY3 is greatly acknowledged.

Appendix A

For a beam consisted of k segments with different cross-sectional properties, e.g. flexural stiffness $(EI)_i$ and linear mass density m_i, using Euler–Bernoulli's beam model the governing differential equation of the ith segment can be written as:

$$(EI)_i \frac{\partial^4 y_i}{\partial x^4} + m_i \frac{\partial^2 y_i}{\partial t^2} = 0, \quad x_i < x < x_{i+1}, \;\; i = 1, 2, \ldots, k \tag{A.1}$$

In case of the helical spring segment, the equivalent flexural stiffness derived in the previous sections were adopted in Eq. (A.1). Otherwise, the ordinary definition of flexural stiffness of a beam was employed for the segment. By using the separation of variables: $y_i(x,t) = w_i(x)e^{j\omega t}$ and rewriting the governing equation as:

$$\frac{\partial^4 w_i}{\partial x^4} - \lambda_i^4 w_i = 0, \quad x_i < x < x_{i+1}, \;\; i = 1, 2, \ldots, k, \tag{A.2}$$

where

$$\lambda_i^4 = \frac{m_i \omega^2}{(EI)_i}, \tag{A.3}$$

the general solution of the deflection function w_i becomes,

$$w_i(x) = A_i \sin \lambda_i(x - x_i) + B_i \cos \lambda_i(x - x_i) + C_i \sinh \lambda_i(x - x_i) + D_i \cosh \lambda_i(x - x_i). \tag{A4}$$

Herein, A_i, B_i, C_i and D_i denote the integration constants for this ith segment. If the joining between the ith and $(i+1)$th segment is perfect, the following continuities both in displacements and reactions should be satisfied:

$$w_i(x_{i+1}^-) = w_{i+1}(x_{i+1}^+), \tag{A.5a}$$

$$w_i'(x_{i+1}^-) = w_{i+1}'(x_{i+1}^+), \tag{A.5b}$$

$$(EI)_i w_i''(x_{i+1}^-) = (EI)_{i+1} w_{i+1}''(x_{i+1}^+), \tag{A.5c}$$

$$(EI)_i w_i'''(x_{i+1}^-) = (EI)_{i+1} w_{i+1}'''(x_{i+1}^+). \tag{A.5d}$$

Substituting the deflections w_i and w_{i+1} into the above equations, a relationship between integration constants for the ith and (i+1)th segment can be established:

$$\begin{Bmatrix} A_{i+1} \\ B_{i+1} \\ C_{i+1} \\ D_{i+1} \end{Bmatrix} = [T]_{(i)} \begin{Bmatrix} A_i \\ B_i \\ C_i \\ D_i \end{Bmatrix}. \tag{A.6}$$

The components of the 4×4 transfer matrix $[T]_{(i)}$ are as following:

$$T_{11} = \frac{1}{2}\left[\frac{\lambda_i}{\lambda_{i+1}} + \frac{(EI)_i}{(EI)_{i+1}}\left(\frac{\lambda_i}{\lambda_{i+1}}\right)^3\right]\cos\,\lambda_i L_i, \quad T_{12} = -\frac{1}{2}\left[\frac{\lambda_i}{\lambda_{i+1}} + \frac{(EI)_i}{(EI)_{i+1}}\left(\frac{\lambda_i}{\lambda_{i+1}}\right)^3\right]\sin\,\lambda_i L_i$$

$$T_{13} = \frac{1}{2}\left[\frac{\lambda_i}{\lambda_{i+1}} - \frac{(EI)_i}{(EI)_{i+1}}\left(\frac{\lambda_i}{\lambda_{i+1}}\right)^3\right]\cosh\,\lambda_i L_i, \quad T_{14} = \frac{1}{2}\left[\frac{\lambda_i}{\lambda_{i+1}} - \frac{(EI)_i}{(EI)_{i+1}}\left(\frac{\lambda_i}{\lambda_{i+1}}\right)^3\right]\sinh\,\lambda_i L_i$$

$$T_{21} = \frac{1}{2}\left[1 + \frac{(EI)_i}{(EI)_{i+1}}\left(\frac{\lambda_i}{\lambda_{i+1}}\right)^2\right]\sin\,\lambda_i L_i, \quad T_{22} = \frac{1}{2}\left[1 + \frac{(EI)_i}{(EI)_{i+1}}\left(\frac{\lambda_i}{\lambda_{i+1}}\right)^2\right]\cos\,\lambda_i L_i$$

$$T_{23} = \frac{1}{2}\left[1 - \frac{(EI)_i}{(EI)_{i+1}}\left(\frac{\lambda_i}{\lambda_{i+1}}\right)^2\right]\sinh\,\lambda_i L_i, \quad T_{24} = \frac{1}{2}\left[1 - \frac{(EI)_i}{(EI)_{i+1}}\left(\frac{\lambda_i}{\lambda_{i+1}}\right)^2\right]\cosh\,\lambda_i L_i$$

$$T_{31} = \frac{1}{2}\left[\frac{\lambda_i}{\lambda_{i+1}} - \frac{(EI)_i}{(EI)_{i+1}}\left(\frac{\lambda_i}{\lambda_{i+1}}\right)^3\right]\cos\,\lambda_i L_i, \quad T_{32} = -\frac{1}{2}\left[\frac{\lambda_i}{\lambda_{i+1}} - \frac{(EI)_i}{(EI)_{i+1}}\left(\frac{\lambda_i}{\lambda_{i+1}}\right)^3\right]\sin\,\lambda_i L_i$$

$$T_{33} = \frac{1}{2}\left[\frac{\lambda_i}{\lambda_{i+1}} + \frac{(EI)_i}{(EI)_{i+1}}\left(\frac{\lambda_i}{\lambda_{i+1}}\right)^3\right]\cosh\,\lambda_i L_i, \quad T_{34} = \frac{1}{2}\left[\frac{\lambda_i}{\lambda_{i+1}} + \frac{(EI)_i}{(EI)_{i+1}}\left(\frac{\lambda_i}{\lambda_{i+1}}\right)^3\right]\sinh\,\lambda_i L_i$$

$$T_{41} = \frac{1}{2}\left[1 - \frac{(EI)_i}{(EI)_{i+1}}\left(\frac{\lambda_i}{\lambda_{i+1}}\right)^2\right]\sin\,\lambda_i L_i, \quad T_{42} = \frac{1}{2}\left[1 - \frac{(EI)_i}{(EI)_{i+1}}\left(\frac{\lambda_i}{\lambda_{i+1}}\right)^2\right]\cos\,\lambda_i L_i$$

$$T_{43} = \frac{1}{2}\left[1 + \frac{(EI)_i}{(EI)_{i+1}}\left(\frac{\lambda_i}{\lambda_{i+1}}\right)^2\right]\sinh\,\lambda_i L_i, \quad T_{44} = \frac{1}{2}\left[1 + \frac{(EI)_i}{(EI)_{i+1}}\left(\frac{\lambda_i}{\lambda_{i+1}}\right)^2\right]\cosh\,\lambda_i L_i \tag{A.7}$$

This transformation relation based on the continuity at the joint between segments can be applied sequentially and a final transfer matrix can be obtained for a k-segment beam:

$$\begin{Bmatrix} A_k \\ B_k \\ C_k \\ D_k \end{Bmatrix} = [T]_{(k-1)}[T]_{(k-2)}\cdots[T]_{(1)} \begin{Bmatrix} A_1 \\ B_1 \\ C_1 \\ D_1 \end{Bmatrix} = [T] \begin{Bmatrix} A_1 \\ B_1 \\ C_1 \\ D_1 \end{Bmatrix}. \tag{A.8}$$

Finally, the boundary conditions of the beam have to be enforced. For instance, if the beam is in cantilevered configuration, the associated boundary conditions read:

$$w_1(0) = 0, \tag{A.9a}$$

$$w_1'(0) = 0, \tag{A.9b}$$

$$w_k''(L) = 0, \tag{A.10a}$$

$$w_k'''(L) = 0. \tag{A.10b}$$

The boundary conditions at $x = 0$ are the vanishing of the deflection and the slope. Substituting these two constraints into the deflection function for the first segment, we arrive at the following equations:

$$B_1 + D_1 = 0, \tag{A.11}$$

$$A_1 + C_1 = 0. \tag{A.12}$$

Hence,

$$\begin{Bmatrix} A_1 \\ B_1 \\ C_1 \\ D_1 \end{Bmatrix} = \begin{bmatrix} 1 & 0 \\ 0 & 1 \\ -1 & 0 \\ 0 & -1 \end{bmatrix} \begin{Bmatrix} A_1 \\ B_1 \end{Bmatrix} \tag{A.13}$$

At the free end of the cantilever beam $x = L$, the equations for the vanishing of the shear force and bending moment take the following matrix form:

$$\begin{bmatrix} -\sin \lambda_k L_k & -\cos \lambda_k L_k & \sinh \lambda_k L_k & \cosh \lambda_k L_k \\ -\cos \lambda_k L_k & \sin \lambda_k L_k & \cosh \lambda_k L_k & \sinh \lambda_k L_k \end{bmatrix} \begin{Bmatrix} A_k \\ B_k \\ C_k \\ D_k \end{Bmatrix} = \begin{Bmatrix} 0 \\ 0 \end{Bmatrix}. \tag{A.14}$$

Taking the integration constants from Eq. (A.8) into the above equations and then the boundary constraint equations from Eq. (A.13), we can arrive at the homogeneous equations with the reduced transfer matrix:

$$[T_R] \begin{Bmatrix} A_1 \\ B_1 \end{Bmatrix} = \begin{Bmatrix} 0 \\ 0 \end{Bmatrix}, \tag{A.15}$$

where

$$[T_R] = \begin{bmatrix} -\sin \lambda_k L_k & -\cos \lambda_k L_k & \sinh \lambda_k L_k & \cosh \lambda_k L_k \\ -\cos \lambda_k L_k & \sin \lambda_k L_k & \cosh \lambda_k L_k & \sinh \lambda_k L_k \end{bmatrix} [T] \begin{bmatrix} 1 & 0 \\ 0 & 1 \\ -1 & 0 \\ 0 & -1 \end{bmatrix}. \tag{A.16}$$

For nontrivial solutions of the integration constants, the determinant of the reduced transfer matrix $[T_R]$ must be singular. This vanished determinant can be used to find the natural frequencies of the beam. A bisection method was employed in this study to locate the natural frequency within a specified frequency span. Accordingly, the associated mode shape can be found by substituting the integration constants back into the deflection functions with the corresponding natural frequency ω.

References

[1] W.Y. Huang, C.P. Chao, J.R. Kang, C.K. Sung, The application of ball-type balancers for radial vibration reduction of high-speed optic disk drives, *Journal of Sound and Vibration* 250 (3) (2001) 415–430.

[2] Y. Takatoshi, Disk Drive Device, Japanese Patent 10,188,465, 1998.

[3] K. Masaaki, Disk Device, Japanese Patent 10,208,374, 1998.

[4] Y. Jinnouchi, Y. Araki, J. Inoue, Y. Ohtsuka, C. Tan, Automatic balancer (static balancing and transient response of a multi-ball balancer), *Transactions of the Japan Society of Mechanical Engineers Part C* 59 (557) (1993) 79–84.

[5] H.C. Zhou, C.Y. Lee, C.K. Sung, The study on the ER suspension system used in the vibration reduction of optical disk drive, *The Proceedings of the 13th R.O.C. Conference on the Vibration and Acoustics*, June 5, Yuan-lin, Taiwan, Paper No. B9 (2005) (in Chinese).

[6] W.H. Wong, P.C. Tse, K.J. Lau, Y.F. Ng, Spring constant of fibre-reinforced plastics circular springs embedded with nickel–titanium alloy wire, *Composite Structures* 65 (2004) 319–328.

[7] K. Williams, G. Chiu, R. Bernhard, Adaptive-passive absorbers using shape-memory alloys, *Journal of Sound and Vibration* 249 (2002) 835–848.

[8] C. Liang, C.A. Rogers, Design of shape memory alloy springs with applications in vibration control, *Journal of Vibration and Acoustics* 115 (1993) 129–135.
[9] V. Yildirim, An efficient numerical method for predicting the natural frequencies of cylindrical helical springs, *International Journal of Mechanical Sciences* 41 (1999) 919–939.
[10] J.E. Mottershead, Finite elements for dynamical analysis of helical rods, *International Journal of Mechanical Sciences* 22 (1980) 267–283.
[11] L.E. Becker, G.G. Chassie, W.L. Cleghorn, On the natural frequencies of helical compression springs, *International Journal of Mechanical Sciences* 44 (2002) 825–841.
[12] J. Lee, Free vibration analysis of cylindrical helical springs by the pseudospectral method, *Journal of Sound and Vibration* 302 (2007) 185–196.
[13] A.P. Boresi, O.M. Sidebottom, *Advanced Mechanics of Materials*, Wiley, Taiwan, 1985.
[14] W.C. Hurty, M.F. Rubinstein, *Dynamics of Structures*, Prentice-Hall, New Jersey, 1964.
[15] H.P. Lin, S.C. Chang, J.D. Wu, Beam vibrations with arbitrary number of cracks, *Journal of Sound and Vibration* 258 (5) (2002) 987–999.
[16] S. Naguleswaran, Natural frequencies, sensitivities and mode shape details on an Euler–Bernoulli beam with one step change in cross-section and with ends on classical supports, *Journal of Sound and Vibration* 252 (4) (2002) 751–767.